REVIEW

Hydroxyapatite nanocrystals: colloidal chemistry, assembly and their biological applications

Junfeng Hui[a,b] and Xun Wang*[b]

Hydroxyapatite (HAp) nanocrystals with excellent biocompatibility and bioresorbability are usually used in the fields of tissue engineering, medicine, etc. In this review, recent advances in the tunable synthesis, ion doping, assembly and applications of monodisperse HAp nanocrystals are summarized, which may be helpful for the designed synthesis and surface modification of HAp or other nanocrystals according to practical applications.

1. Introduction

As the main constituent of inorganic phase in the human body, hydroxyapatite (HAp) has excellent biocompatibility, bioresorbability, osteogenesis, osteoconductivity and osteo-inductivity, and easily forms direct chemical bonds with living tissue.[1–4] Therefore, HAp plays extremely important and irreplaceable roles in the field of tissue engineering. In order to endow other materials with excellent biological and mechanical properties, HAp nanocrystals are often used as coating materials and inorganic phase of organic/inorganic composites.[5–8] HAp has many other applications. HAp spheres can be used as nano-carriers for controlled drug delivery.[9] Nanoscale HAp could selectively inhibit the growth of cancer cells and is expected to become novel green anticancer drugs.[10–12] In addition, HAp is a good medium to separate and purify sugars, amino acids, peptides, nucleic acids, enzymes, proteins, and other biological macromolecules in the non-acidic system.[13–15] HAp powder can be used as a water treatment agent to remove heavy metal ions such as Cd^{2+}, Hg^{2+}, and Pb^{2+} based on ion-exchange reaction.[16,17] HAp is usually used in catalysis as supporting material. Recently, HAp was found to be an inexpensive and effective phase-pure catalyst for volatile organic compound combustion.[18]

*a*Shaanxi Key Laboratory of Degradable Biomedical Materials, Shaanxi R&D Center of Biomaterials and Fermentation Engineering, School of Chemical and Engineering, Northwest University, Xi'an, 710069, P. R. China
*b*Department of Chemistry, Tsinghua University, Beijing, 100084, P. R. China. E-mail: wangxun@mail.tsinghua.edu.cn

Associate Professor Junfeng Hui received his Ph.D. degree in Bio-chemical Engineering from Northwest University in 2010, followed by working with Prof. Xun Wang in Department of Chemistry, Tsinghua University as a postdoctoral fellow. He joined the faculty of Chemical Engineering School, Northwest University after his undergraduate study in 1998, and was promoted to associate professor in 2011. His main awards include the second prize for the National Award for Technological Invention (2013). His current research interests focus on the preparation and application of functional nanometer materials.

Junfeng Hui

Professor Xun Wang received his Ph.D. degree from the Department of Chemistry, Tsinghua University in 2004. Then he joined the faculty of the Department of Chemistry, Tsinghua University as a research assistant, and was promoted to associate professor and full professor in 2005 and 2007, respectively. His main awards include National Science and Technology Award for Young Scientist (2009), National Science Fund for Distinguished Young Scholars (2007) and IUPAC Prize for Young Chemists (2005). His current research interests include synthetic methodology, self-assembly and properties of inorganic nanocrystals.

Xun Wang

This journal is © the Partner Organisations 2014

Inorg. Chem. Front., 2014, **00**, 1–11 | 1

Fig. 1 LSS strategy for nanocrystal synthesis. Adapted with permission from ref. 31, Copyright 2005, Nature Publishing Group.

Up to now, many methods have been reported for the preparation of HAp, such as (microwave-) hydrothermal, homogeneous precipitation, sol–gel, electrophoretic deposition, microemulsion, the template method, the solid phase method, and biomineralization.[19–27] HAp with various shapes, sizes, stoichiometries, and levels of crystallinity can be obtained, depending on the synthetic technique. Foreign-ion doping further enriches the kinds and properties of HAp and extends their potential applications. For example, europium ions will endow HAp crystals with bright fluorescence properties,[28] and silver or zinc ion doping makes HAp crystals have antimicrobial and catalytic properties.[29,30]

HAp particles in native bone are nanoscale platelets or rods.[1,2] However, most of the preparation of HAp crystals is fulfilled in the water phase, and the resulting particle size is relatively too large, and/or prone to aggregate, limiting their effective application. The controlled synthesis of monodisperse hydroxyapatite nanocrystals is a continuing focus.

Herein, we mainly summarize our recent endeavor on the synthesis, assembly and application of monodisperse HAp nanorods, nano-spindles, nanowires, etc. The whole summary consists of four parts. Firstly, Liquid-Solid-Solution (LSS) phase transfer and separation strategy[31] is interpreted and applied in the preparation of HAp nanorods and fluorine-substituted (FHAp) nanotubes. Secondly, based on this or a modified strategy, synthesis and properties of monodisperse ion-doped HAp nanocrystals are reviewed. Thirdly, we describe the (self-) assembly of several kinds of monodisperse HAp nanocrystals and analyze the related mechanism of assembly. Finally, we introduce surface grafting modification and encapsulation methods, by which hydrophobic HAp nanocrystals are converted into hydrophilic ones. Meanwhile, the corresponding biological application experiment is described.

2. LSS phase transfer and separation strategy

In 2005, Wang et al. first presented a LSS phase transfer synthetic strategy for the synthesis of various functional nanocrystals with different chemistries and properties.[31] As shown in Fig. 1, the LSS strategy reveals actually an oil–water interface-controlled reaction system which refers to three phases (liquid, solid, and solution phase) and two interfaces (liquid–solid and solid–solution interface). In this system, water, ethanol, long chain fatty acid and its metal-salt form a relatively complex three-phase reaction system: a water–ethanol mixed solution acts as the main continuous solution phase dissolving starting inorganic salts, ethanol and long chain fatty acid (like oleic acid or linoleic acid) serve as a liquid phase, and fatty acid metal salt (sodium linoleate, sodium oleic acid, and so on) is a solid phase. Under the designated reaction conditions, the M^{n+} ions of $(RCOO)_nM$ could be reduced to metal nanocrystals by ethanol, or dehydrate to oxides and/or composite oxides, or react with other anion species from solution phase to yield a large variety of functional nanocrystals.[32–39] The as-obtained
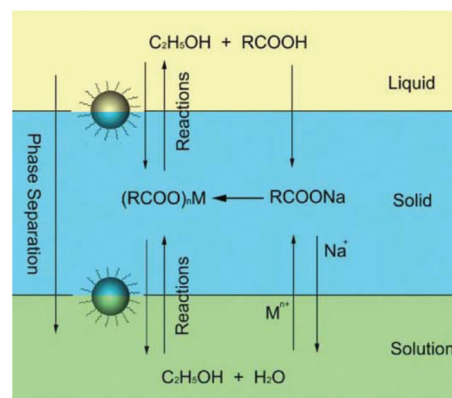
product will be easily collected because of a spontaneous phase-separation process based on the weight of nanocrystals and/or incompatibility between their hydrophobic surfaces and hydrophilic surroundings. This strategy has been demonstrated to be effective in the synthesis of HAp nanocrystals with controllable sizes and shapes comparable with those of other colloidal nanocrystals.

2.1 LSS strategy for the synthesis of monodisperse HAp nanorods

Based on this LSS strategy, Wang et al. successfully fabricated uniform monodisperse HAp nanorods with tunable sizes, aspect ratios, and surface properties at 80–200 °C for about 8–10 h.[40] As shown in Fig. 2, sodium linoleate (or sodium oleate), linoleic acid (or oleic acid), and ethanol were mixed together under agitation; then an aqueous solution of $Ca(NO_3)_2$ was added to form the liquid (ethanol/linoleic acid), solid (sodium linoleate), and solution ($Ca(NO_3)_2$ aqueous solution) phases. After the ion-exchange process of Ca^{2+} and Na^+, a solution of Na_3PO_4 was added to the solution phase and reacted with the calcium linoleate. The as-obtained Hap
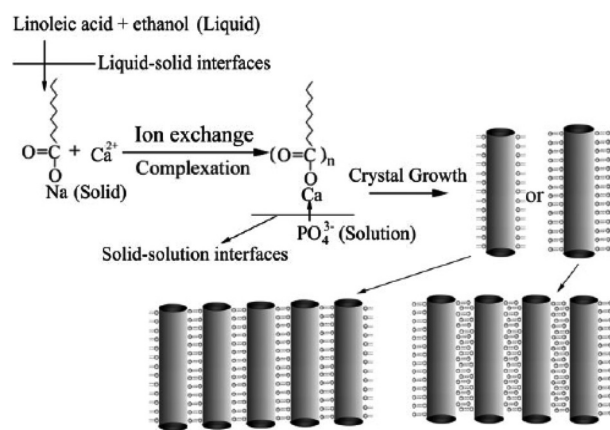

Fig. 2 LSS strategy to HAp nanorods and their assembly. Adapted with permission from ref. 40, Copyright 2006, Wiley Online Library.

2 | Inorg. Chem. Front., 2014, 00, 1–11

This journal is © the Partner Organisations 2014

nanocrystals have highly uniform sizes and narrow size- and length-distributions. By tuning the reaction temperatures, the surface properties can be further controlled, and the experimental results show that the HAp nanorods possess stable hydrophobic surface properties under higher-temperature conditions based on monolayer complexation of linoleic acid on the outer surface, or unstable hydrophilic ones under lower-temperature conditions which were attributed to the bilayer absorption of linoleic acid on the surfaces.

2.2 Synthesis of FHAp nanotubes based on Kirkendall effect

Compared with nanorods, single-crystal nanotube structures have better mechanical properties.[41–45] Based on the LSS process and Kirkendall effect, Hui *et al.* synthesized monodisperse single-crystal F-substituted HAp (FHAp) nanotubes with different aspect ratios *via* a hydrothermal-based synthetic method (Fig. 3a–i).[46] It was found that uniform nanotubes can be obtained when F^- ions were added to the system before PO_4^{3-} ions; in contrast, only nanorods with small pores on the surfaces can be obtained if PO_4^{3-} ions were added before F^- ions. The possible process was that Ca^{2+} ions and F^- ions first generate CaF_2, and then the CaF_2 react with the absorbed PO_4^{3-} ions to form CaF_2 @ HAp. CaF_2 gradually vanished with F^- doped into the HAp lattice, so hollow interior space was left with the formation of nanotubes. The TEM images from the as-obtained nanotubes revealed that with the increase of F/Ca molar ratios from 0.033 to 0.25, the aspect ratios of HAp nanotubes would decrease, and the diameters would increase from

10 to 20 nm when the lengths decreased from 200 to 50 nm. Further study showed that the addition of the amphiphilic ligand polyethylene glycol (PEG, higher than 10 000, MW) into the reaction system would lead to formation of nanotubes with amphiphilic surface properties, which was attributed to the co-anchoring of PEG and hydrophobic oleic acid on the outer surface of the nanotubes.

F doping into the lattice of HAp will certainly improve their anti-erosion performance. To investigate the stability of FHAp nanotubes and pure HAp nanorods synthesized in the LSS system, they were immersed in the mixed solution of acetic acid and water for a certain period of time. The results showed that HAp nanorods were quickly destroyed and converted into dicalcium phosphate dihydrate (DCPD) hollow nanospheres with diameters of about 10–60 nm, while the structures of FHAp nanotubes remained nearly the same as before erosion.[46,47] All these indicate that these FHAp nanotubes are quite stable in acidic environments.

3. Doping chemistry of HAp nanocrystals

3.1 Rare-earth doped FHAp nano-spindles and/or nanowires

Rare-earth element doping was proved to be effective in the preparation of novel functional nanomaterials, which not only can effectively control the growth of the nanocrystals, but also endow the product with abundant performance for potential applications, such as optical communication, display devices, catalysis, biological labeling, *etc.*[48–56] For the mixed solvent system of octadecylamine, oleic acid and water, different rare-earth ions (La^{3+}, Ce^{3+}, Nd^{3+}, Eu^{3+}, Gd^{3+}, Tb^{3+}, Er^{3+}, Tm^{3+}, Yb^{3+}, *etc.*) and F^- ions are chosen as doping ions. We found that the reaction temperature, pH value, and volume ratio of the mixed solvent were crucial to synthesize HAp nanostructures with different morphologies and properties. As shown in Fig. 4, when the mixture of 4 mL oleic acid, 16 mL ethanol, about 16 mL water and 0.5 g octadecylamine was used as the reaction system, and $Ca(NO_3)_2 \cdot 4H_2O$, Na_3PO_4, NaF, and rare-earth nitrates were used as starting materials, FHAp:Ln^{3+} (Ln = Ce, Eu, Tb, *etc.*) nano-spindles were easily prepared. The increasing amount of fluorine ions led to smaller length-to-diameter ratios of the nano-spindles, and the increasing amount of rare-earth ions contributed to the preparation of nano-spindles with more sharp heads.[57] In our previous work, rice-like FHAp nanocrystals were once reported as the intermediate in the process of crystal growth.[46] Herein, it was apparent that the absorption of octadecylamine on the surface and the doping of rare-earth ions suppressed the growth along the *c*-axis and resulted in the formation of rice-like end-product. The experimental results also showed that the anion surfactants oleic acid could be preferable for the growth along the *c*-axis and rare-earth ions could further enhance the template function of oleic acid because of their higher positive charge than calcium ions in the absence of octadecylamine. As shown in Fig. 5, when choosing the mixture of 20 mL of oleic acid, 8 mL of
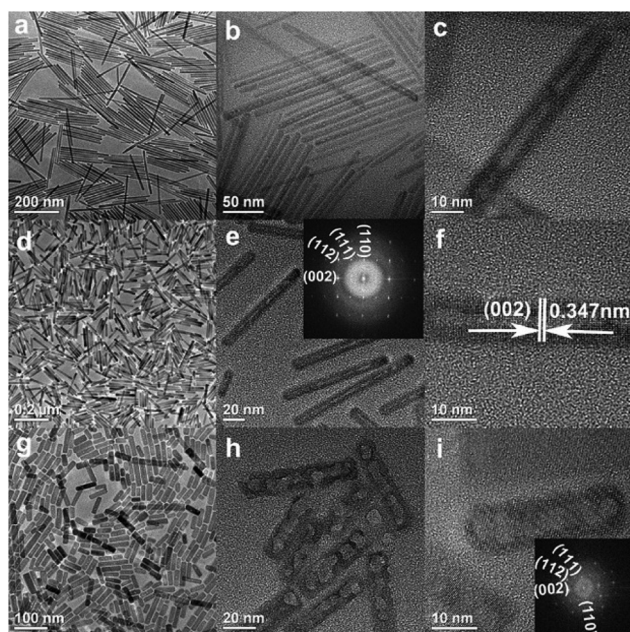

Fig. 3 (a–i) Representative TEM and HRTEM images of FHAp nanotubes with different doping levels: a–c, F/Ca = 0.033, 100 °C; d–f, F/Ca = 0.05, 100 °C; g–i, F/Ca = 0.25, 100 °C. (j) Variance of lengths and diameters of nanotubes with the difference in the F/Ca ratio. (k) IR spectra taken from F-HAp nanotubes with different doping levels. Adapted with permission from ref. 46, Copyright 2009, American Chemical Society.
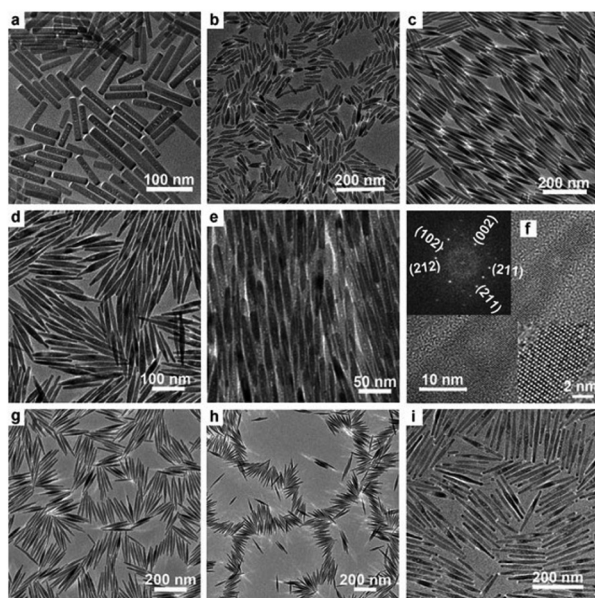
Fig. 4 Representative TEM and HRTEM images of FHAp nanoparticles with different doping levels (molar ratio) in the reaction system composed of octadecylamine, oleic acid, ethanol, and water (F/Ca = 0.2, 150 °C, 12 h for all samples): (a) Eu/Ca = 0, (b) Eu/Ca = 2.5 : 97.5, (c–f) Eu/Ca = 5 : 95, (g) Tb/Ca = 5 : 95, (h) Ce/Ca = 5 : 95, and (i) Er/Ca = 20 : 80. The inset in (f) shows a local enlargement of the HRTEM image (bottom right corner) and the corresponding Fourier-transform diffractogram (top left corner). Adapted with permission from ref. 57, Copyright 2011, Wiley Online Library.

Fig. 6 Luminescent spectra of rice-like FHAp-Eu^{3+} nanoparticles under different doping conditions: (a) 5% Eu^{3+} at 220 °C (green line), 180 °C (blue line), 150 °C (red line), and 120 °C (black line); (b) 10% Eu^{3+} (green line), 5% Eu^{3+} (blue line), 2.5% Eu^{3+} (red line), and 1% Eu^{3+} (black line). The inset in (a) shows the ordinary (left) and luminescent (right) photographs of FHAp-Eu^{3+} (5%) nanoparticles (180 °C, 12 h) dissolved in cyclohexane. (c) Luminescent spectra of rice-like FHAp-Tb[3+] nanoparticles with different Tb[3+]-doping levels: 10% (green line), 5% (red line), 2.5% (blue line), and 1% (black line). The inset in (c) shows the fluorescence photograph of FHAp-Tb[3+] (5%) nanoparticles (180 °C, 12 h) dissolved in cyclohexane. (d) The fluorescence micrograph of FHAp-Eu^{3+} powder shown in the inset in (a). Adapted with permission from ref. 57. Copyright 2011, Wiley Online Library.

ethanol, 9 mL of water, and the right amount of NaOH as the reaction system, and Ca(NO$_3$)$_2$·4H$_2$O, Na$_3$PO$_4$, NaF, and rare-earth nitrates were likewise used as starting materials, the end-product could be dramatically tuned from rice-like nanocrystals to single-crystal ultrathin nanowires with diameters 3–4 nm and lengths up to 5–10 μm.[57] The ionic radius of the Ln[3+] ion is close to that of the Ca^{2+} ion, which well proved that different rare-earth elements would lead to similar results in the same reaction systems.

Studies have shown that the doping of Eu^{3+} (or Tb[3+]) ions usually makes nanocrystals have novel optical properties.[58,59] In the doping experiments as described above, FHAp:Eu^{3+} (or Tb[3+]) nano-spindles were endowed with bright red (or green) luminescence properties (Fig. 6).[57] It was clear that the replacement of –OH groups in the lattice by F^{−} ions could lessen the hydroxyl-quenching effects on the photoluminescence properties and significantly enhance the luminescence properties of the nanocrystals. In addition, the reaction temperature and the doping amount of Eu^{3+} (or Tb[3+]) ions strongly affected the fluorescence properties of the as-obtained materials. However, it was worth noting that the HRTEM images of nano-spindles and ultrathin nanowires show that they all grow along the c-axis corresponding with the (002) lattice plane and were highly crystalline (Fig. 4f and 5g), and the former possessed better fluorescence intensity than the latter, when adopting the same conditions of temperature, reaction time, and the molar ratio of raw materials.
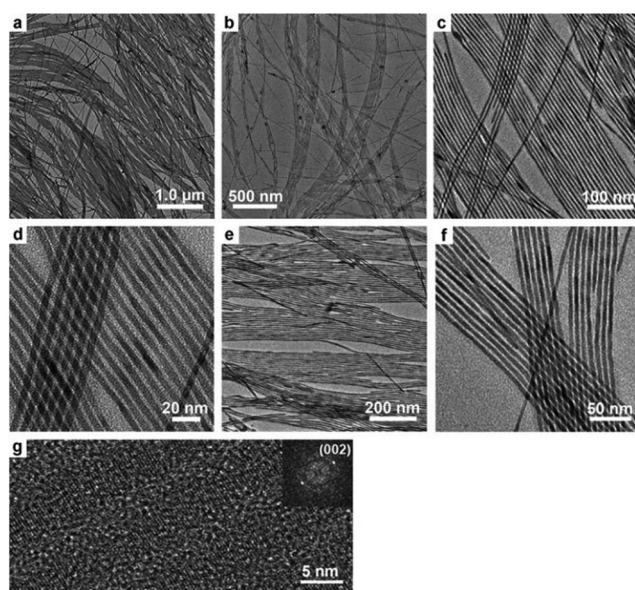

Fig. 5 Representative TEM and HRTEM images of FHAp nanowires with different doping levels (molar ratio) at 180 °C for 36 h in the reaction system composed of NaOH, oleic acid, ethanol, and water: (a–d) 10% Yb[3+], (e) 10% Er[3+], (f) 10% Tm[3+] (F/Ca = 0.2, Ln[3+] doping percent based on the total molar number of Ca and Ln[3+]). (g) HRTEM image and the corresponding Fourier-transform diffractogram (inset) of the nanowires shown in (a)–(d). Adapted with permission from ref. 57. Copyright 2011, Wiley Online Library.
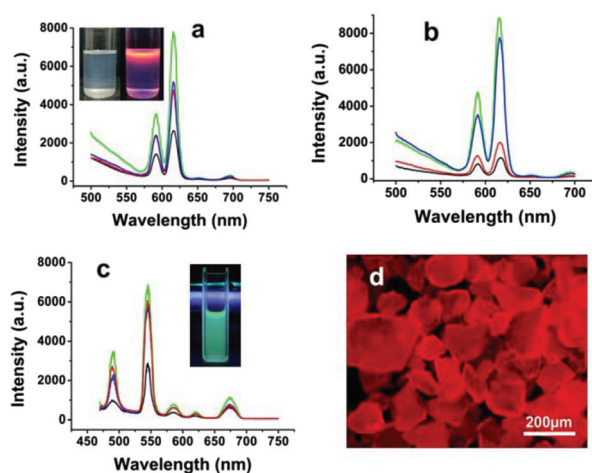
3.2 Ultrathin CHAp nanowires and their full color emission by rare earth doping

In the natural bone mineral, HAp nanocrystals are not pure and contain about 4–8 wt% of carbonate and other ionic substitutions like Na^+, Mg^{2+}, K^+, F^-, Cl^-, and so on. According to the hydroxyapatite structure, the carbonate group can easily substitute both the hydroxyl and the phosphate ions of the HAp crystal lattice, and form A-type and B-type carbonated hydroxyapatite (CHAp), respectively.[60–62] CHAp nanocrystals are characterized by the low stability and high reactivity which meet the needs of the organism.[62]

To simulate natural biological minerals in the structure characteristics and further investigate the mutual influence between PO_4^{3-} and CO_3^{2-} groups in the synthesis of nano-crystals, abundant carbonate ions were introduced into the reaction system in the preparation of HAp nanoparticles.[63] The results displayed that the reaction temperature and P/C (PO_4^{3-}/CO_3^{2-}) molar ratios of precursors were the main factors that influenced the structures of the final products. With the same reaction temperature (90–220 °C), time and Ca/C (Ca^{2+}/CO_3^{2-}) molar ratios of 1, increasing the P/C molar ratios in the reaction system would gradually tune the diameter from ∼1 to 4 nm and length from 200 to 800 nm of the as-obtained CHAp solid-solution ultrathin nanowires (Fig. 7).

Perhaps because of the existence of abundant HAp unit cells, in which the PO_4^{3-} and OH^- ions were replaced by CO_3^{2-}, the ultrathin CHAp solid-solution nanowires obtained in the suitable P/C molar ratio could produce bright self-activated blue luminescence (Fig. 8a).[63–66] If the ultrathin CHAp nano-wires were chosen as the matrix and doped with Tb^{3+} or Eu^{3+} ions by the second hydrothermal synthesis process, the as-prepared CHAp:Eu^{3+} (or Tb^{3+}) nanowires with unchanged morphology could emit bright green (red) luminescence (Fig. 8b and c). Using the above tricolors of ultrathin nano-wires, recombination luminescence over a full-color spectrum range was easily obtained (Fig. 8d and e).[63] Fig. 9 shows TEM images and the corresponding EDS analysis of the ultrathin CHAp:Eu^{3+} (or Tb^{3+}) nanowires prepared by a two-step process.

3.3 Ultrathin CHAp/Ln³⁺ solid-solution nanowires

In the same system containing oleic acid, octadecylamine, ethanol and deionized water, we succeeded in synthesizing ultrathin CHAp:Ln^{3+} (Ln = Ce, Eu, Tb) nanowires of about 1 nm diameter and 10–300 nm length by suitably tuning the doping amount of the rare-earth ions *via* a one-step approach, which further pushed the size of the CHAp nanobuilding blocks to one unit cell region (Fig. 10).[63] FTIR spectra demonstrated that the rare-earth-doped ultrathin nanowires also have the same characteristic peaks similar to the CHAp nanocrystals as reported in the literature (Fig. 11A).[60] It showed that the co-doping synergy of different foreign ions could easily cause the growth malformation of the original matrix and lead to the formation of novel ultrathin nanostructures.
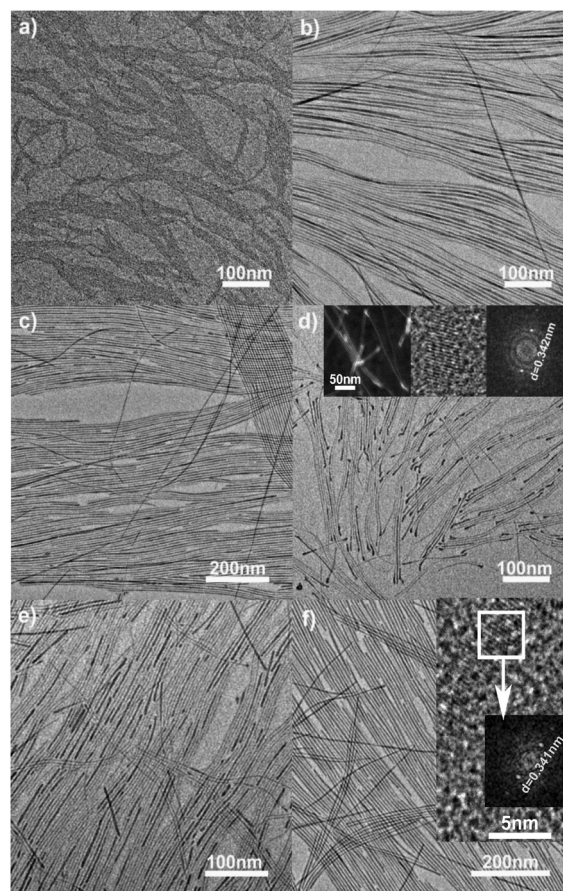

Fig. 7 TEM images of the ultrathin CHAp solid-solution nanowires under different conditions. (a, b) 90 °C, 12 h, the P/C molar ratios of 9 and 36%; (c) 150 °C, 12 h, the P/C molar ratio of 30%. (d–f) 220 °C, 12 h, the P/C molar ratios were 6, 12 and 30%, respectively. Inset in (d), STEM image of nanowires (left), HRTEM image of the bulky nanowire end (middle), and the corresponding Fourier-transform diffractogram (right). Inset in (f), HRTEM image of the nanowires and the corresponding Fourier-transform diffractogram. Adapted with permission from ref. 63. Copyright 2012, Wiley Online Library.

4. Assembly of monodisperse HAp nanocrystals

The *in vivo* complex hierarchical macrostructures with multi-functions like bone, muscle fiber, lipid bilayer, *etc.* are all perfectly assembled by different levels of tiny units.[67] The rapidly developing electron microscopy technique reveals how the fascinating magic structures happen. Inspired by these assembly phenomena of micro/nanoscale units, scientists have been especially keen on researching the assembly and performances of various elementary building blocks.[68–70] Due to interesting shape- and size-dependent phenomena and properties, the self-assembly and potential applications of nanocrystals have been extensively investigated in catalysis, sensing, energy storage, electronics, tissue engineering, medicine, environment, *etc.*[71–79] The bottom-up strategy is usually implemented by the assembly of basic nanoscale blocks (such as nanorods,
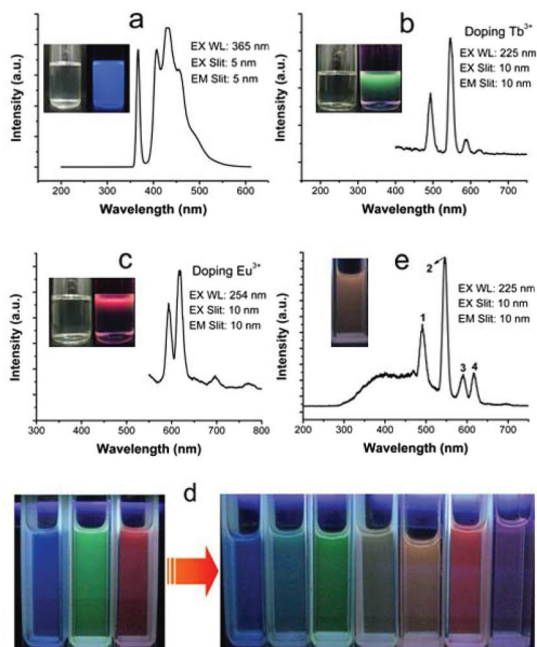
This journal is © the Partner Organisations 2014

Inorg. Chem. Front., 2014, 00, 1–11 | 5

Fig. 8 (a)–(c) Fluorescence spectra of three ultrathin CHAp nanowires formed under different doping conditions (Ln/Ca molar ratio: none, 10% Tb^{3+}, and 10% Eu^{3+}, respectively); insets: the nanowire solution in cyclohexane under visible light (left) and under UV light (right). (d) Full-color images of the three fluorescent solutions (left) and their mixtures (right). (e) Fluorescence spectra and photograph (inset) of a mixture of the green and red fluorescent solutions. Fluorescent photographs were taken under λ = 254 nm UV light by using a camera. Adapted with permission from ref. 63. Copyright 2011, Wiley Online Library.
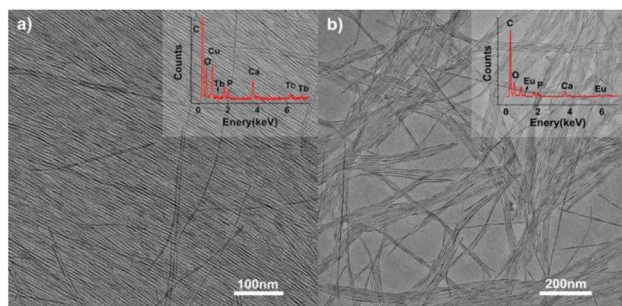

Fig. 9 TEM images of ultrathin CHAp solid-solution nanowires doped with (a) Tb^{3+} ions and (b) Eu^{3+} ions. Inset: the corresponding EDS analysis. Adapted with permission from ref. 63. Copyright 2012, Wiley Online Library.

Fig. 10 TEM images of the ultrathin CHAp/Ln^{3+} solid-solution nanowires synthesized through a one-step hydrothermal process at 120 °C for 12 h. Precursor: CO_3^{2-} (7 mL), Ca^{2+} (7 − x) mL, PO_4^{3-} 0.35 mL, x is the doping ions, as follows: (a) Ce^{3+} (0.7 mL), (b) Ce^{3+} (0.8 mL), (c) Eu^{3+} (0.35 mL), (d) Eu^{3+} (0.7 mL), (e) Tb^{3+} (0.14 mL), (f) Tb^{3+} (0.35 mL). Adapted with permission from ref. 63. Copyright 2012, Wiley Online Library.

nanowires, nanotubes, and nanopolyhedra) into expected macro/nanostructures. Compared with single atoms or molecules and the bulk counterparts, individual nanocrystals show different properties and become excellent building blocks. But this usually requires precise control over the nanocrystals themselves in terms of size, shape, concentration, monodispersity and the medium in which they are suspended.[70]

The LSS strategy is not only a general method of monodisperse nanocrystal synthesis, and but also of surface modificatio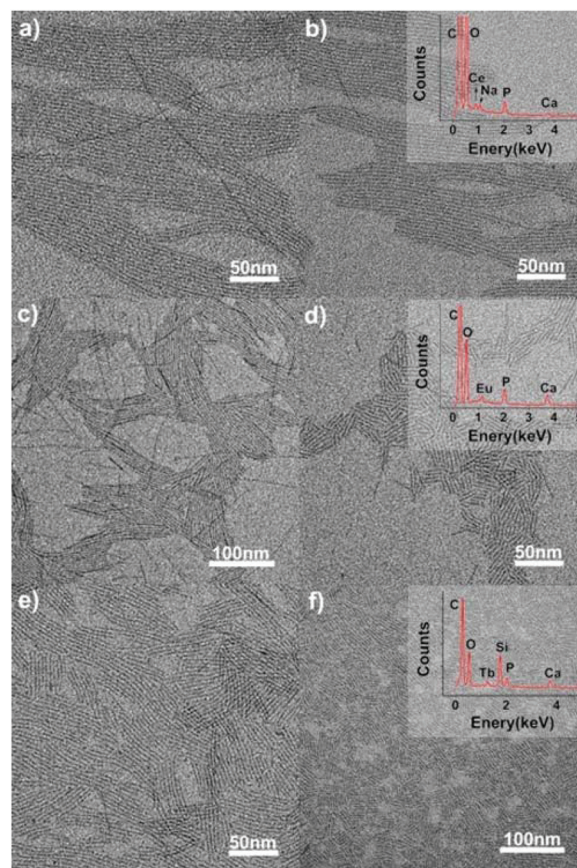n of nanocrystals prone to self-assembly. Using universal LSS methods, Wang and his colleagues have synthesized different kinds of nanocrystals and found that specific shapes and long-chain ligand modified surfaces are two key factors to direct the self-assembly of functional nanocrystals into higher-order superstructures, and the interactions between the long-chain ligands on the crystal surface would induce the crystal to assemble into certain patterns.[80,81] For example, Hu et al. availed a mixture of oleic acid, oleylamine, ethanol and water to synthesize new kinds of one-dimensional ultrathin nanostructures of rare earth hydroxide.[80] Through the reduction of size and the increased ratio of ligand to inorganic backbone, the as-synthesized ultrathin nanoribbons with thicknesses less than 1 nm could self-assemble into series of interesting space conformations (nanoloops, periodic frameworks, and various coiling conformations) based on the interaction and energy balance among organic ligands, inorganic structure, and solvent, with reduced flexural rigidity of ultrathin nanowires and/or nanoribbons.

In the process of HAp nanocrystals synthesized *via* the LSS strategy, the self-assembly phenomenon of the different
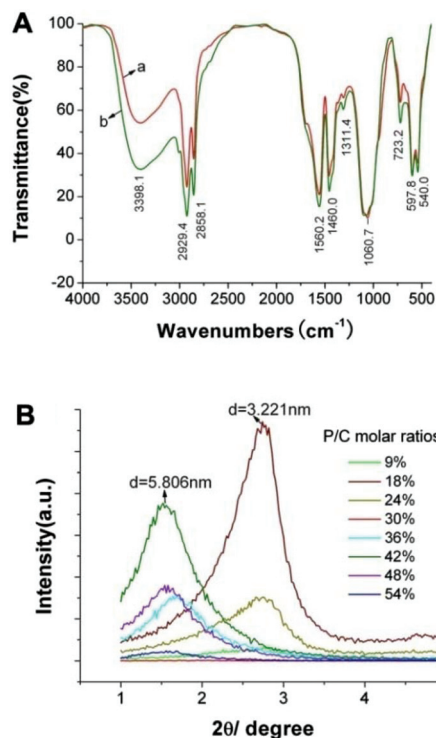
Fig. 11 (A) FTIR spectrum of the as-prepared ultrafine CHAp solid-solution nanowires doped with (a) Ce^{3+} or (b) Tb^{3+}; (B) SXRD patterns of the ultrathin CHAp solid-solution nanowires obtained with different P/C molar ratios at 90 °C for 12 h. Adapted with permission from ref. 63, Copyright 2012, Wiley Online Library.

Fig. 12 Ce^{3+}-doped nanowires in cyclohexane (left) and a film formed from Ce^{3+}-doped nanowires (right). Adapted with permission from ref. 63, Copyright 2012, Wiley Online Library.
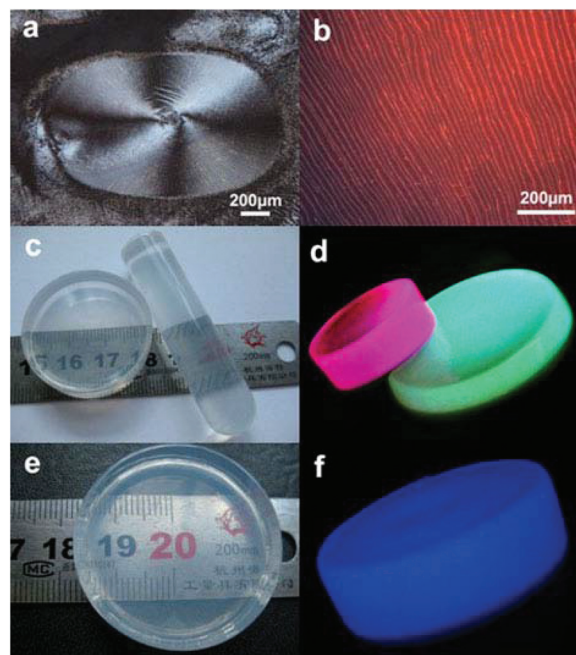

Fig. 13 (a) and (b) show micrographs of dark-field and green-light excitation of a thin layer formed on glass slides from droplets of FHAp:Eu^{3+} nanoparticles dissolved in cyclohexane; (c) photograph that shows the physical dimensions and the transparency of the nanoparticle/poly (dimethylsiloxane) PDMS composite materials composed of FHAp:Eu^{3+} (5%, left) and FHAp:Tb^{3+} (5%, right) nanoparticles; (d) fluorescence photograph of the PDMS samples obtained by a camera through excitation with UV light at 254 nm; (e) photograph showing physical dimension and transparency of the nanowire/PDMS composite material; (f) fluorescence photograph of the nanowire/PDMS sample taken under λ = 254 nm UV light by using a camera. Adapted with permission from ref. 57 and 63, Copyright 2011, 2012, Wiley Online Library.

morphologies of nanocrystals was also very common. On the carbon-coated copper grids, HAp nanorods, FHAp nanotubes, FAp:Ln^{3+} nanospindles (FAp refers to FHAp with doping levels of F/Ca = 0.2) and ultrathin nanowires tended to form parallel arranged bundles with adjacent nanocrystals along with increasing concentration (Fig. 2–5, 7, 8 and 10).[40,46,57,63] The phenomenon should be attributed to the fact that the as-prepared nanocrystals were all enshrouded in a layer of oleic acid, and the interactions between abundant ligands in the surface resulted in the regular arrangements of nanocrystals with even intervals. Fig. 11B shows small angle X-ray diffraction (SXRD) patterns of the ultrathin CHAp solid-solution nanowires obtained with different P/C molar ratios at 90 °C for 12 h.[63] The SXRD patterns had different response peaks corresponding to the layer spacing and relative evenness of the samples, which entirely reflected the uniformity of the obtained samples and the thickness of hydrophobic capping layer (oleic acid and/or octadecylamine) with about 0.9–1.1 nm.

Gradual concentration of monodisperse nanocrystals at the interface is the most basic process for generation of reference assemblies. Various techniques aiming at the interfaces are developed, such as drop casting evaporation, sedimentation, and substrate-induced evaporation, *etc.* which are convenient for assembly of nanocrystals.[82–85] About 1 nm CHAp:Ce^{3+} solid-solution nanowires could easily form transparent film

even through the simple centrifugal sedimentation and natural dry process (Fig. 12).[83] And when FAp:Eu^{3+} nanospindles cyclohexane solutions were dropped on the glass slide, the nanospindles would self-assemble into neat stripe patterns by cyclohexane evaporation (Fig. 13a and b).[57]

In addition, all kinds of as-obtained HAp nanocrystals have excellent hydrophobic surface, uniform sizes and shapes, and could perfectly assemble with a hydrophobic polymer. As shown in Fig. 4, FAp:Ln^{3+} (Ln = Eu or Tb) nanospindles, CHAp or CHAp:Ln^{3+} nanowires could be successfully assembled into the PDMS with different shapes which did not influence the

polymerization of polymers and endowed the new materials with perfect luminescent properties (Fig. 13c–f).[57,63] Undoubtedly, the above co-assembly of PDMS-HAp means the realization of more complexities with more functions and flexibilities.

5. Biological applications of HAp nanocrystals

HAp nanocrystals are usually used in the field of tissue engineering, medicine and health, industrial catalysis, environmental protection and other important aspects.[11,15–18,59,61] HAp nanocrystals are good host materials and usually doped with diverse ions like Mg^{2+}, Zn^{2+}, Sr^{2+}, Fe^{2+}, Eu^{3+}, Tb^{3+}, F^-, Cl^-, CO_3^{2-}, *etc.* The ion-doped HAp nanoparticles are often endowed with many new changes such as shape and size, optical and/or magnetic properties, catalysis, and so on. In general, the synthesis of hydroxyapatite is implemented in the water phase system, and it is difficult to control the shape and size of particles, to a certain extent, limiting their application because of the large particle scale. Our research group adopted the LSS strategy to synthesize pure or ion-doped HAp nanocrystals with hydrophobic surfaces, which greatly enriched the types, features and application of nanometer HAp, such as the preparation of PDMS-HAp composite materials with luminescent properties. But the super-hydrophobic surfaces of HAp nanocrystals also hamper their potential application in the hydrophilic environment.

In order to achieve the hydrophobic/hydrophilic conversion, several strategies were frequently adopted, as the following: oxidation of the oleic acid capping ligand into azelaic acids $(HOOC(CH_2)_7COOH)$ by Lemieux–von Rudloff reagent,[86–88] the complete exchange of the oleic acid molecule with a hydrophilic ligand like poly(acrylicacid) (PAA),[88] and polymer encapsulation.[78] Hui *et al.* successfully converted hydrophobic nanocrystals into hydrophilic ones *via* surface grafting modification using a surfactant (Pluronic F127).[89] Fig. 14 shows the representative surfactant-mediated hydrophobic/hydrophilic transformation of fusiform FAp:Eu^{3+} nanocrystals for the purpose of cell markers. The as-prepared uniform hydrophilic
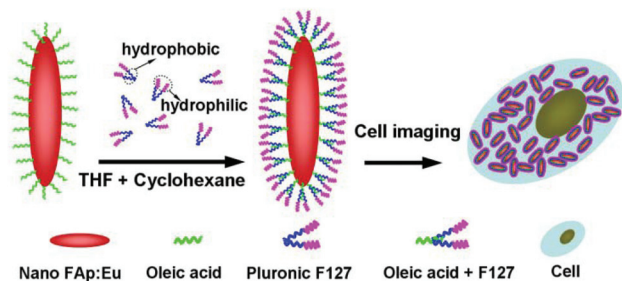

Fig. 14 Schematic showing transformation of oleic acid coated fluoridated HAp:Eu^{3+} nanoparticles to hydrophilic fluorescent nanocrystals with Pluronic F127 and their use as cell imaging probes. Adapted with permission from ref. 89, Copyright 2012, the Royal Society of Chemistry.
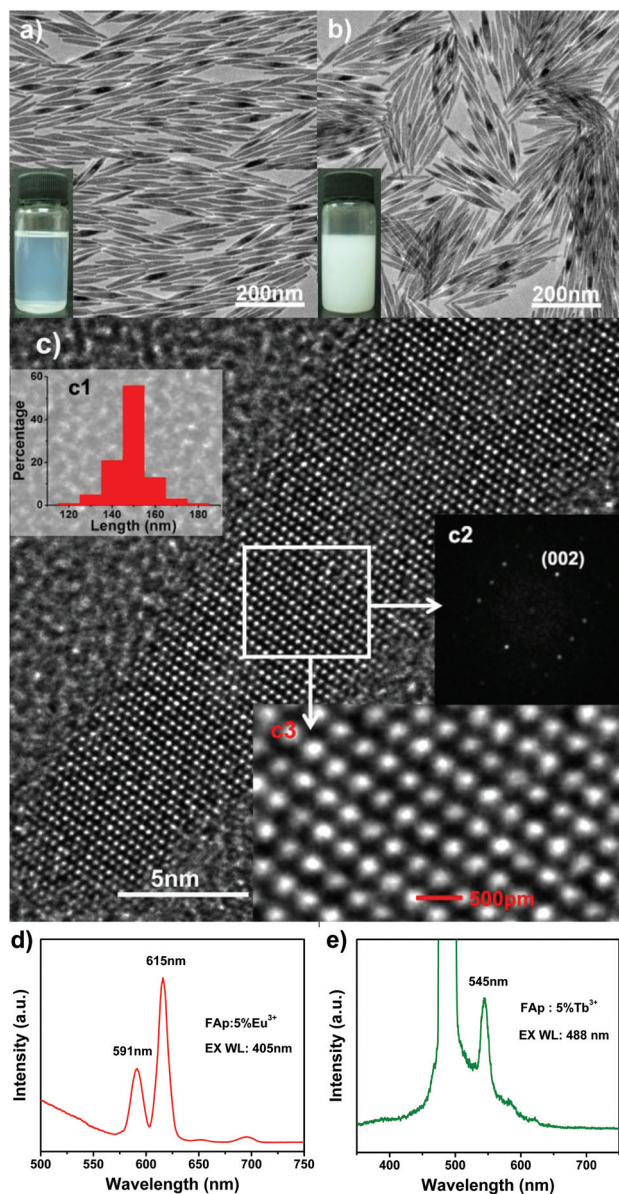

Fig. 15 (a) TEM image of the hydrophobic FAp:5%Eu^{3+} nanoparticles, the inset shows nanoparticles dissolved in cyclohexane under room light. (b) TEM image of the hydrophilic FAp:5%Eu^{3+} nanoparticles, the inset shows nanoparticles dissolved in water under room light. (c) HRTEM image of the FAp:5%Eu^{3+} nanoparticles in (a); insets in (c) are the corresponding length distribution (c1) of nanoparticles, Fourier–transform diffractogram (c2) and local enlargement (c3) of HRTEM images, respectively. (d) Luminescent spectrum of the FAp:5%Eu^{3+} nanoparticles under excitation at 405 nm. (e) Luminescent spectrum of the FAp:5% Tb[3+] nanoparticles under excitation at 488 nm. Adapted with permission from ref. 89, Copyright 2011, the Royal Society of Chemistry.

FAp:Eu^{3+} nanospindles with good crystallinity could be very well dispersed in aqueous solution, as well as in cyclohexane solution before modification, as shown in Fig. 15a–c. The hydrophilic FAp:Eu^{3+} (or Tb[3+]) nanocrystals would not significantly change the luminescence emission of them (Fig. 15d and e). The results of A549 cells and HeLa cells cultured in
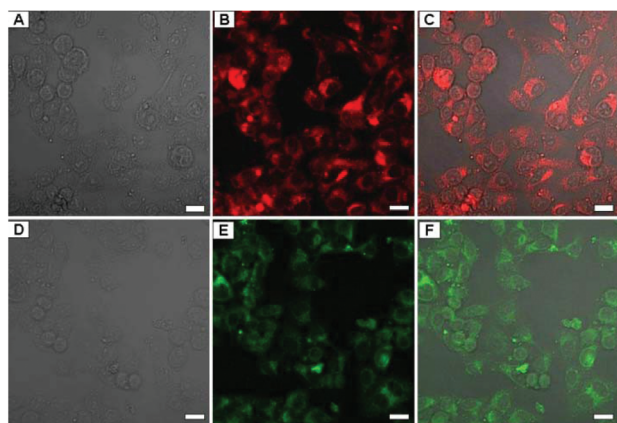
8 | *Inorg. Chem. Front.*, 2014, **00**, 1–11

This journal is © the Partner Organisations 2014

Fig. 16 LCSM images of A549 cells incubated with 150 μg mL^{-1} of FAp-PEG nanorods for 3 h. (A–C) FAp:Eu^{3+}-PEG nanorods, (D–F) FAp:Tb^{3+}-PEG nanorods; (A and D) bright field, (B and E) fluorescent images excited with a 405 nm (Eu) and a 488 nm (Tb) laser, and (C and F) merged images. Scale bar = 20 μm. Adapted with permission from ref. 90, Copyright 2013, the Royal Society of Chemistry.

media containing different concentrations of FAp:Eu^{3+} (or Tb^{3+}) nanocrystals demonstrated that these nanoparticles had excellent biocompatibility.

In addition, Zhang *et al.* proposed a novel PEGylation strategy for surface modification of FAp:Eu^{3+} (or Tb^{3+}) nanorods with diblock synthetic polymers.[90] Choosing stearyl methacrylate (SMA) and poly(ethylene glycol)methacrylate (PEGMA) as monomers, Zhang *et al.* synthesized amphiphilic polymers through reversible addition-fragmentation chain transfer (RAFT) polymerization. When the aqueous solution of amphiphilic polymers and the cyclohexane solution of FAp:Eu^{3+} (or Tb^{3+}) nanorods were added into a suitable amount of tetrahydrofuran, the hydrophobic segments (SMA) readily interacted with the oleic acid on the nanorods. After removing the organic media by rotary evaporation, hydrophilic FAp:Eu^{3+} (or Tb^{3+}) nanorods with PEG coating could be prepared. These PEGylated FAp:Eu^{3+} (or Tb^{3+}) nanorods maintained the original morphology, possessed excellent biocompatibility and strong red or green fluorescence which was successfully utilized for living cell imaging (Fig. 16).

In order to achieve effective transformation from hydrophobility to hydrophilic properties of HAp:Eu^{3+} nanocrystals and simultaneously enhance their potential applications, Pan *et al.* proposed another different scheme which fabricated novel functional nanomaterials.[91] According to this strategy (Fig. 17A), HAp:Eu^{3+} nanocrystals were encapsulated into biocompatible polymer (poly D,L-lactide-*co*-gly-colide, PLGA) nanospheres with the surface carboxyl groups *via* a solvent extraction/evaporation method, and then the surface of polymer NPs encapsulating HAp:Eu^{3+} nanocrystals were grafted with the targeting molecule (folate). The as-prepared HAp:Eu^{3+}-loaded PLGA nanoparticles with folate decoration can be observed in Fig. 17B and E. Experimental results displayed that the new type of functional NPs had low toxicity, high sensitivity, and good photostability, and they could be
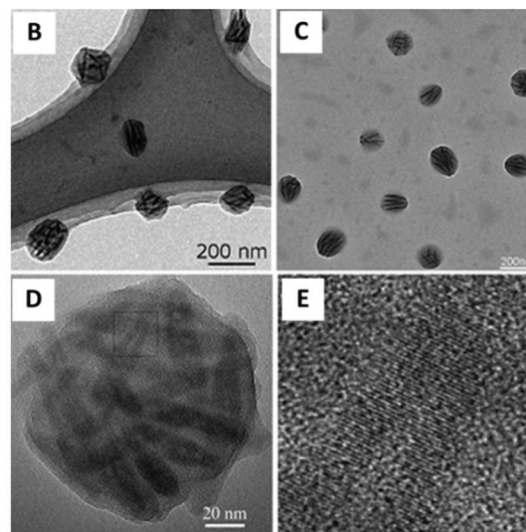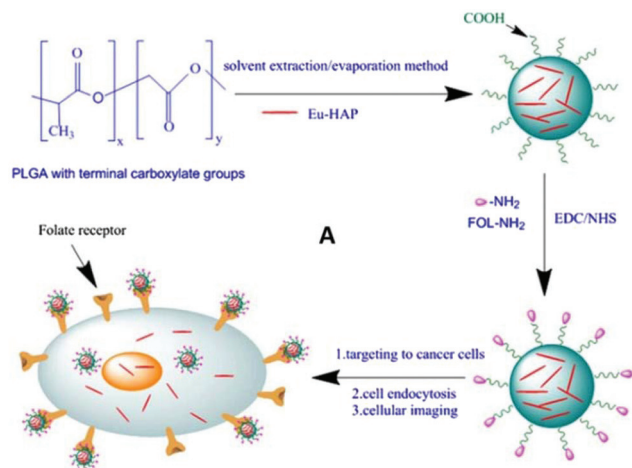

Fig. 17 (A) Detailed scheme for preparation of HAp:Eu^{3+}-loaded nanoparticles with folate decoration for cellular imaging; (B, C) TEM images of HAp:Eu^{3+}-loaded nanoparticles with folate decoration; (D) HRTEM images of a single HAp:Eu^{3+} polymer nanoparticle; (E) enlarged HRTEM image of the square part in D. Adapted with permission from ref. 91, Copyright 2013, American Institute of Chemical Engineers.

used for specific targeted imaging of MCF-7 breast cancer cells with overexpression folate receptors by folate receptor-mediated endocytosis.

6. Conclusions

Over the years, based on excellent physical/chemical properties and biological performance of HAp nanocrystals, their synthesis methods and application ways have been pursued by many researchers. In this article, we summarize our recent developments in tunable synthesis, ion doping, assembly and applications of monodisperse HAp nanocrystals. Through the design of reasonable ligands, types of dopant and doping ways, series of HAp nanocrystals with different shapes/sizes and features were successfully prepared and applied. However,

This journal is © the Partner Organisations 2014

Inorg. Chem. Front., 2014, **00**, 1–11 | 9

there are still many challenges, as the following: how to achieve more precise control of synthesis, how to synthesize hydrophilic ultrathin nanocrystals, how to simulate biological assembly utilizing different nano-HAp building blocks, how to fabricate novel/new HAp nanocrystals by multiple-ion synergistic effect, and so on. We believe that these issues are significant to expand potential application of HAp nanocrystals in biotechnology, catalysis, medicine, *etc.*, and hope that the relevant research process and results can provide reference for the development of other materials.

Acknowledgements

Notes and references

1 M. A. Meyers, P. Y. Chen, A. Y. M. Lin and Y. Seki, *Prog. Mater. Sci.*, 2008, **53**, 1.

2 F. Z. Cui, Y. Li and J. Ge, *Mater. Sci. Eng., R*, 2007, **57**, 1.

3 L. C. Palmer, C. J. Newcomb, S. R. Kaltz, E. D. Spoerke and S. I. Stupp, *Chem. Rev.*, 2008, **108**, 4754.

4 X. Su, K. Sun, F. Z. Cui and W. J. Landis, *Bone*, 2003, **32**, 150.

5 D. M. Liu, Q. Z. Yang and T. Troczynski, *Biomaterials*, 2002, **23**, 691.

6 Y. Yang, K. H. Kim and J. L. Ong, *Biomaterials*, 2005, **26**, 327.

7 L. Zhang, P. Tang, M. Xu, W. Zhang, W. Chai and Y. Wang, *Acta Biomater.*, 2010, **6**, 2189.

8 H. Zhou and J. Lee, *Acta Biomater.*, 2011, **7**, 2769.

9 T. Y. Liu, S. Y. Chen, D. M. Liu and S. C. Liou, *J. Control. Release*, 2005, **107**, 112.

10 M. Corti and F. J. Rohlf, *Biol. J. Linn. Soc.*, 2001, **73**, 99.

11 M. Iafisco, J. M. Delgado-Lopez, E. M. Varoni, A. Tampieri, L. Rimondini, J. Gomez-Morales and M. Prat, *Small*, 2013, **9**, 3834.

12 M. Z. Yin, Y. C. Han, I. W. Bauer, P. Chen and S. P. Li, *Biomed. Mater.*, 2006, **1**, 38.

13 W. Paul and C. P. Sharma, *J. Colloid Interf. Sci.*, 1995, **174**, 224.

14 A. Barroug, J. Fastrez, J. Lemaitre and P. Rouxhet, *J. Colloid Interf. Sci.*, 1997, **189**, 37.

15 Y. Hou, C. J. Morrison and S. M. Cramer, *Anal. Chem.*, 2011, **83**, 3709.

16 S. Saxena and S. F. D'Souza, *Environ. Int.*, 2006, **32**, 199.

17 J. A. Gómez del Rio, P. J. Morando and D. S. Cicerone, *J. Environ. Manage.*, 2004, **71**, 169.

18 J. Xu, T. White, P. Li, C. He and Y. F. Han, *J. Am. Chem. Soc.*, 2010, **132**, 13172.

19 I. Mobasherpour, M. S. Heshajin, A. Kazemzadeh and M. Zakeri, *J. Alloys Compd.*, 2007, **430**, 330.

20 Z. C. Wang, F. Chen, L. M. Huang and C. J. Lin, *J. Mater. Sci.*, 2005, **40**, 4955.

21 N. Nassif, F. Martineau, O. Syzgantseva, F. Gobeaux, M. Willinger, T. Coradin, S. Cassaignon, T. Azaïs and M. M. Giraud-Guille, *Chem. Mater.*, 2010, **22**, 3653.

22 D. M. Liu, Q. Yang, T. Troczynski and W. J. Tseng, *Biomaterials*, 2002, **23**, 1679.

23 J. K. Han, H. Y. Song, F. Saito and B. T. Lee, *Mater. Chem. Phys.*, 2006, **99**, 235.

24 G. C. Koumoulidis, A. P. Katsoulidis, A. K. Ladavos, P. J. Pomonis, C. C. Trapalis, A. T. Sdoukos and T. C. Vaimakis, *J. Colloid Interf. Sci.*, 2003, **259**, 254.

25 G. Guo, Y. Sun, Z. Wang and H. Guo, *Ceram. Int.*, 2005, **31**, 869.

26 Q. Ren, H. J. Luo and L. Zhou, *Rare Metal Mat. Eng.*, 2004, **33**, 115.

27 K. Kandori, T. Kuroda, S. Togashi and E. Katayama, *J. Phys. Chem. B*, 2011, **115**, 653.

28 O. A. Graeve, R. Kanakala, A. Madadi, B. C. Williams and K. C. Glass, *Biomaterials*, 2010, **31**, 4259.

29 V. Stanić, D. Janaćković, S. Dimitrijević, S. B. Tanasković, M. Mitrić, M. S. Pavlović, A. Krstić, D. Jovanović and S. Raičević, *Appl. Surf. Sci.*, 2011, **257**, 4510.

30 G. Liu, J. W. Talley, C. Na, S. L. Larson and L. G. Wolfe, *Environ. Sci. Technol.*, 2010, **44**, 1366.

31 X. Wang, J. Zhuang, Q. Peng and Y. Li, *Nature*, 2005, **437**, 121.

32 X. Wang, J. Zhuang, Z. Huo, S. Hu and Y. Li, *Inorg. Chem.*, 2008, **47**, 543.

33 X. Wang, J. Zhuang, Q. Peng and Y. Li, *Langmuir*, 2006, **22**, 7364.

34 X. Liang, X. Wang, J. Zhuang, Y. Chen, D. Wang and Y. Li, *Adv. Funct. Mater.*, 2006, **16**, 1805.

35 Z. Zhuang, Q. Peng, J. Liu, X. Wang and Y. Li, *Inorg. Chem.*, 2007, **46**, 5179.

36 X. Wang, J. Zhuang, Q. Peng and Y. Li, *Inorg. Chem.*, 2006, **45**, 6661.

37 Z. Huo, C. Chen, D. Chu, H. Li and Y. Li, *Chem.–Eur. J.*, 2007, **13**, 7708.

38 X. Liang, X. Wang, J. Zhuang, Q. Peng and Y. Li, *Adv. Funct. Mater.*, 2007, **17**, 2757.

39 S. Hu, H. Liu, P. Wang and X. Wang, *J. Am. Chem. Soc.*, 2013, **135**, 11115.

40 X. Wang, J. Zhuang, Q. Peng and Y. Li, *Adv. Mater.*, 2006, **18**, 2031.

41 L. Sun, F. Banhart, A. V. Krasheninnikov, J. A. Rodriguez-Manzo, M. Terrones and P. M. Ajayan, *Science*, 2006, **312**, 1199.

42 O. H. Kwon and A. H. Zewail, *Science*, 2010, **25**, 1668.

43 J. Goldberger, R. Fan and P. Yang, *Acc. Chem. Res.*, 2006, **39**, 239.

44 M. R. Falvo, G. J. Clary, R. M. Taylor Li, V. Chi, F. P. Brooks Jr., S. Washburn and R. Superfine, *Nature*, 1997, **389**, 582.

45 S. Hu and X. Wang, *J. Am. Chem. Soc.*, 2008, **130**, 8126.

46 J. Hui, G. Xiang, X. Xu, J. Zhuang and X. Wang, *Inorg. Chem.*, 2009, **48**, 5614.

47 J. Hui and D. Fan, *J. Mater. Res.*, 2009, **24**, 2499.

48 F. Wang, Y. Han, C. S. Lim, Y. Lu, J. Wang, J. Xu, H. Chen, C. Zhang, M. Hong and X. Liu, *Nature*, 2010, **463**, 1061.

49 F. Zhang, J. Li, J. Shan, L. Xu and D. Zhao, *Chem.–Eur. J.*, 2009, **15**, 11010.

50 Y. Liu, D. Wang, J. Shi, Q. Peng and Y. Li, *Angew. Chem., Int. Ed.*, 2013, **52**, 4366.

51 M. A. Katkova and M. N. Bochkarev, *Dalton Trans.*, 2010, **39**, 6599.

52 W. Qin, D. Zhang, D. Zhao, L. Wang and K. Zheng, *Chem. Commun.*, 2010, **46**, 2304.

53 H. Q. Wang, M. Batentschuk, A. Osvet, L. Pinna and C. J. Brabec, *Adv. Mater.*, 2011, **23**, 2675.

54 J. C. Zhou, L. D. Sun, J. Shen, J. Q. Gu and C. H. Yan, *Nanoscale*, 2011, **3**, 1977.

55 D. J. Naczynski, M. C. Tan, M. Zevon, B. Wall, J. Kohl, A. Kulesa, S. Chen, C. M. Roth, R. E. Riman and P. V. Moghe, *Nat. Commun.*, 2013, **4**, 2199.

56 V. Kachkanov, M. J. Wallace, G. van der Laan, S. S. Dhesi, S. A. Cavill, Y. Fujiwara and K. P. O'Donnell, *Sci. Rep.*, 2012, **2**, 969.

57 J. Hui and X. Wang, *Chem.–Eur. J.*, 2011, **17**, 6926.

58 P. Yang, Z. Quan, C. Li, X. Kang, H. Lian and J. Lin, *Biomaterials*, 2008, **29**, 4341.

59 F. Chen, P. Huang, Y. J. Zhu, J. Wu and D. X. Cui, *Biomaterials*, 2012, **33**, 6447.

60 J. Barralet, S. Best and W. Bonfield, *J. Biomed. Mater. Res.*, 1998, **41**, 79.

61 E. Landi, G. Celotti, G. Logroscino and A. Tampieri, *J. Eur. Ceram. Soc.*, 2003, **23**, 2931.

62 S. Padilla, I. Izquierdo-Barba and M. Vallet-Regí, *Chem. Mater.*, 2008, **20**, 5942.

63 J. Hui, Q. Yu, Y. Long, Z. Zhang, Y. Yang, P. Wang, B. Xu and X. Wang, *Chem.–Eur. J.*, 2012, **18**, 13702.

64 A. Pifferi, P. Taroni, A. Torricelli, G. Valentini, P. Mutti, G. Ghislotti and L. Zanghieri, *Appl. Phys. Lett.*, 1997, **70**, 348.

65 M. Fujimaki, Y. Ohki and H. Nishikawa, *J. Appl. Phys.*, 1997, **81**, 1042.

66 C. Zhang, J. Yang, Z. Quan, P. Yang, C. Li, Z. Hou and J. Lin, *Cryst. Growth Des.*, 2009, **9**, 2725.

67 T. Dvir, B. P. Timko, D. S. Kohane and R. Langer, *Nat. Nanotechnol.*, 2011, **6**, 13.

68 E. S. Place, N. D. Evans and M. M. Stevens, *Nat. Mater.*, 2009, **8**, 457.

69 H. B. Yao, H. Y. Fang, X. H. Wang and S. H. Yu, *Chem. Soc. Rev.*, 2011, **40**, 3764.

70 J. X. Gong, G. D. Li and Z. Y. Tang, *Nano Today*, 2012, **7**, 564.

71 S. Sacanna, W. T. M. Irvine, P. M. Chaikin and D. J. Pine, *Nature*, 2010, **464**, 575.

72 M. R. Jones, R. J. Macfarlane, B. Lee, J. Zhang, K. L. Young, A. J. Senesi and C. A. Mirkin, *Nat. Mater.*, 2010, **9**, 913.

73 D. Zerrouki, J. Baudry, D. Pine, P. Chaikin and J. Bibette, *Nature*, 2008, **455**, 380.

74 A. Gautieri, S. Vesentini, A. Redaelli and M. J. Buehler, *Nano Lett.*, 2011, **11**, 757.

75 S. Sacanna, L. Rossi and D. J. Pine, *J. Am. Chem. Soc.*, 2012, **134**, 6112.

76 P. Wang, Y. Yang, J. Zhuang and X. Wang, *J. Am. Chem. Soc.*, 2013, **135**, 6834.

77 Z. Tang, S. Shen, J. Zhuang and X. Wang, *Angew. Chem.*, 2010, **122**, 4707.

78 A. Sánchez-Iglesias, M. Grzelczak, T. Altantzis and B. Goris, *ACS nano*, 2012, **6**, 11059.

79 M. E. Leunissen, R. Dreyfus, R. Sha, T. Wang, N. C. Seeman, D. J. Pine and P. M. Chaikin, *Soft Matter*, 2009, **5**, 2422.

80 S. Hu, H. Liu, P. Wang and X. Wang, *J. Am. Chem. Soc.*, 2013, **135**, 11115.

81 J. F. Liu and Y. D. Li, *Adv. Mater.*, 2007, **19**, 1118.

82 T. Ming, X. Kou, H. Chen, T. Wang, H. L. Tam, K. W. Cheah, J. Y. Chen and J. Wang, *Angew. Chem., Int. Ed.*, 2008, **120**, 9831.

83 A. R. Tao, D. P. Ceperley, P. Sinsermsuksakul, A. R. Neureuther and P. Yang, *Nano Lett.*, 2008, **8**, 4033.

84 J. Huang, F. Kim, A. R. Tao, S. Connor and P. Yang, *Nat. Mater.*, 2005, **4**, 896.

85 Z. Zhu, H. Meng, W. Liu, X. Liu, J. Gong, X. Qiu, L. Jiang, D. Wang and Z. Tang, *Angew. Chem., Int. Ed.*, 2011, **123**, 1631.

86 Z. Chen, H. Chen, H. Hu, M. Yu, F. Li, Q. Zhang, Z. Zhou, T. Yi and C. Huang, *J. Am. Chem. Soc.*, 2008, **130**, 3023.

87 G. Wang, Q. Peng and Y. Li, *J. Am. Chem. Soc.*, 2009, **131**, 14200.

88 R. Naccache, F. Vetrone, V. Mahalingam, L. A. Cuccia and J. A. Capobianco, *Chem. Mater.*, 2009, **21**, 717.

89 J. Hui, X. Zhang, Z. Zhang, S. Wang, L. Tao, Y. Wei and X. Wang, *Nanoscale*, 2012, **4**, 6967.

90 X. Zhang, J. Hui, B. Yang, Y. Yang, D. Fan, M. Liu, L. Tao and Y. Wei, *Polym. Chem.*, 2013, **4**, 4120.

91 J. Pan, D. Wan, Y. Bian, H. Sun, C. Zhang, F. Jin, Z. Huang and J. Gong, *AIChE J.*, 2013, **59**, 4494.